Deformable Octahedron Burrowing Robot

Conference Paper · July 2012

DOI: 10.7551/978-0-262-31050-5-ch057

3 authors, including:

Juan Cristobal Zagal
University of Chile
63 PUBLICATIONS **923** CITATIONS

SEE PROFILE

Shuguang Li
Massachusetts Institute of Technology
32 PUBLICATIONS **1,867** CITATIONS

SEE PROFILE

Deformable Octahedron Burrowing Robot

Juan Cristobal Zagal[1], Cristobal Armstrong[1] and Shuguang Li[2]

[1]Department of Mechanical Engineering, University of Chile, Santiago, Chile
[2]School of Astronautics, Northwestern Polytechnical University, Xi'an, Shaanxi, P.R. China
jczagal@ing.uchile.cl

Abstract

This paper explores the use of a deformable octahedron robot as an alternative for the autonomous exploration of complex confined spaces, voids and tunneling structures. Current robotic platforms lack the capabilities for adapting their shape when moving through intricate sections of cavities. We discuss the geometrical and dynamical properties of a deformable octahedral platform. We use real and simulated robots to test and synthesize locomotion controllers that allow our robots to travel along different portions of a tunneling test bed. Evolutionary methods allow us to automatically produce controllers for in-pipe motion. We demonstrate the capabilities of peristaltic locomotion, different modes of deformation and volumetric adaptation. An evaluation of motion capabilities inside pipe elbows and branches is performed. Our results suggest that this type of deformable robot has a potential for travelling along confined spaces.

Introduction

Current robots have limited capabilities to access confined spaces such as narrow caves, complex pipeline networks, bifurcating blood vessels and uncharted pipeline networks. Various machines have been proposed for autonomous navigation under confinement. In-pipe robots include wheeled, caterpillar, wall-press, inchworm, screw, walking and even snake-like [19] devices. Flexible catheters have been also developed for robotically assisted surgery [8] as well as many caterpillar-like platforms for disaster and mine exploration [5].

Although robotics snakes and catheters can curve, most devices lack of the capability to deform and shift their shape adapting to the various geometries that might arise under confinement. Deformation seems to be an important capability to be further developed for the autonomous exploration of confined spaces that arise in mines, the human body, collapsed buildings, industrial and marine pipelines, etc.

Although legged animals are successful at travelling over relatively flat terrain (horse, cheetah, etc.), soft deformable invertebrates such as worms, slugs and leeches are the masters of confinement. Earthworms are able to travel underground by exploiting waves of muscular contractions that alternatively shorten and lengthen different portions of their body. Since the shortened part also widens, it can be anchored to the surrounding soil, allowing the narrowed lengthened part to move forward, following a peristaltic pattern [16].

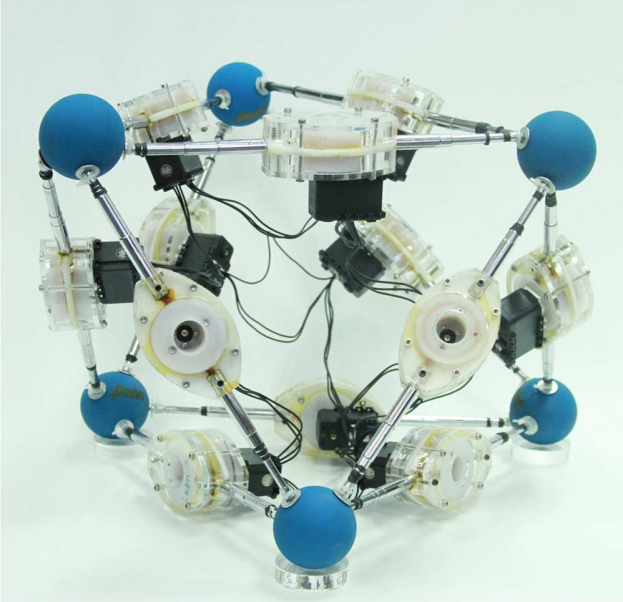

Figure 1: The octahedron burrowing robot. Edges are composed by linear actuators and the vertices are covered by rubber balls used as anchoring material.

The recently expanding literature on deformable robotics illustrates interesting developments on materials, methods, path planning and locomotion of deformable robots, usually on flat terrain. Less attention has been devoted to exploring the applications of these concepts to the exploration of confined environments.

Rather than exploring rugged planar terrain, deformable robots might have a great potential for traveling inside voids and confined spaces. In this study the goal is to explore the capabilities of a deformable octahedron robot to penetrate, travel and transition between cavities and tunneling structures.

Our first prototype uses hydraulic linear actuators and the second was constructed with motorized electric linear actuators, constructed by spinning a drum loaded with a plastic line, following the same principle of power car antennas.

The remainder of this paper is organized as follows: The next section introduces related work, and then the octahedron platform is introduced together with its simulation. Force

feedback is analyzed as well as studies of locomotion inside various pipeline joints. Finally the conclusions are presented.

Related Work

Deformable robots

The ability to significantly deform, adapt and expand, at a much higher level than conventional robotics, enables soft robots to access environments today restricted to conventional autonomous machines. It appears that nature has provided soft animals with extraordinary abilities to control their body even with few muscles and little dedicated neural circuitry [17].

Complex, yet coordinated, motor interactions are apparently obtained from the dynamical coupling between locally regulated muscular structures, enabling organisms to perform control tasks that would otherwise be attributed to centralized neural computation. This ability is related to the recently conceptualized terms of morphological communication [18] and morphological computation [15], where the mechanism itself is used as a form of mind.

The remarkable capabilities of crawling and jumping by a mostly circular soft robot were recently demonstrated in [22]. Active continuous deformation allowed the structure to locomote over rough terrain. Deformation was achieved by extending or shrinking eight shape memory alloy (SMA) coils distributed along the circular perimeter. Due to the high driving voltage and power required by these actuators, the device was tethered during experiments.

Peristaltic locomotion in soft robotics has been demonstrated with different materials. A flexible braided mesh-tube was wrapped with a network of antagonistic NiTi coil actuators in [21]. The prototype, inspired by the hydrostatic skeleton of the Oligochaeta worm, demonstrated robust tethered locomotion over a planar horizontal surface. Interestingly, locomotion persisted after impacts with a hammer were applied to the mechanism.

Soft pneumatic actuators were used in [3], demonstrating how selective inflation of multiple cells along a worm-like body can generate peristaltic motion. The soft cells were constructed using two layers of silicone: a flat layer embedding a fabric mesh, and a thicker expandable layer that produces bimorph bending of the compound when inflated.

The same selective inflation principle was applied by arranging the cells as a circular belt. The resulting ring was able to roll autonomously on a flat surface. Similarly, a peristaltic pattern of motion was also achieved by combining three pneumatic McKibben actuators in series [11]. Their prototype for an autonomous peristaltic endoscope was tested inside a horizontal tube with slight curvature and slope.

Snake-like robots that exhibit peristaltic locomotion have been analyzed in studies like [12,20]. Forward locomotion capabilities are usually studied but less attention has been paid to exploring rotation and volumetric adaptation to the various geometries that might arise in cavities. Turning patterns over the plane were analyzed for the case of a peristaltic robot studied in [13].

Tensegrity and Lattice Robots

Deformable tensegrity robots are composed of an actuated group of struts and cables. A network of struts under pure compression is supported by a continuous network of cables under tension, defining a stable volume in space. Structural morphing is achieved when varying the length of cables or struts. The shape-shifting capabilities of tensegrities enable them to locomote [7].

Tensegrities are highly deployable structures, capable of occupying a large volume when extended or a small space when contracted. They can bend themselves while their constituent elements do not experience any bending torque, since they are only subject to axial forces. When subjected to stress, the structural members are unidirectionally loaded, without reversals in the direction of member load [23]. These properties allow the simplification of element design and control.

The design and control of planar tensegrity models was studied in [6]. Controllers were generated to achieve robust performance and stabilization in the context of manipulation. Design methodologies were given to meet dynamical stiffness and vibration isolation specifications. The design and control for locomotion of more complex tridimensional tensegrities was studied in [14].

Tetrahedral robots are another form of lattice-based deformable robotics, which have mainly been explored for aerospace applications. In [4], the space-filling properties of tetrahedral robots are highlighted as an alternative for mobility on irregular terrain. However, locomotion experiments reported with this type of robot are restricted to planar surfaces [1,2]. They have demonstrated locomotion by tumbling tetrahedra over irregular, but mostly planar, terrain. It is suggested that these robots also have good capabilities for traveling over terrain with high slopes and varying obstacle sizes.

Odin is a great example of a deformable lattice modular robot specification [10]. Rather than defining a particular configuration, Odin defines a set of modules (joint, telescopic actuator and passive rod) that can be used for the construction of arbitrary deformable lattice geometries. Some experiments are reported on basic motion capabilities of a robot constructed using such modular specification. Unfortunately, the robot is hardly reproducible due to the high module cost.

Octahedron Robot

Octahedron Geometry

An octahedron is a polyhedron having eight faces. A regular octahedron belongs to the Platonic solids family. It is made by eight equilateral triangles; four triangles meet at each one of its six vertices. An octahedron has 12 edges. Figure 2 shows an illustration of a planar deployment of a regular octahedron together with different 3D views of the same solid geometry. A deformable octahedron has very interesting space filling properties which enable it to be an excellent platform for the exploration of cavities.

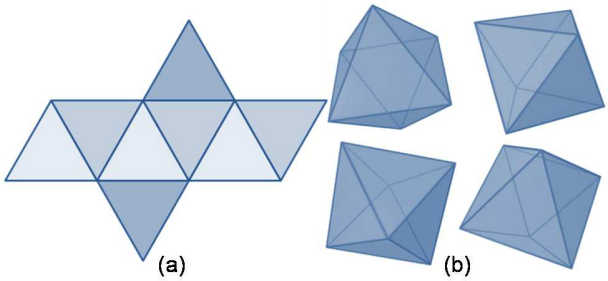

Figure 2: a, planar deployment of a regular octahedron. **b**, different views of the same regular octahedron.

Simulation Model

We implemented a physical simulation of the octahedron robot using the Open Dynamics Engine (ODE). The simulation contains twelve linear actuators serving as the edges of a polyhedron. Four linear actuators meet at each vertex having ball type ODE joints as motion constraints. PID dynamic compensators were used to control the force applied to each actuator while following an actuator length reference signal. The simulation allows investigating shape shifting and locomotion caused when varying the lengths of the platform edges. Figure 3 shows our simulation model under the canonical equilateral configuration.

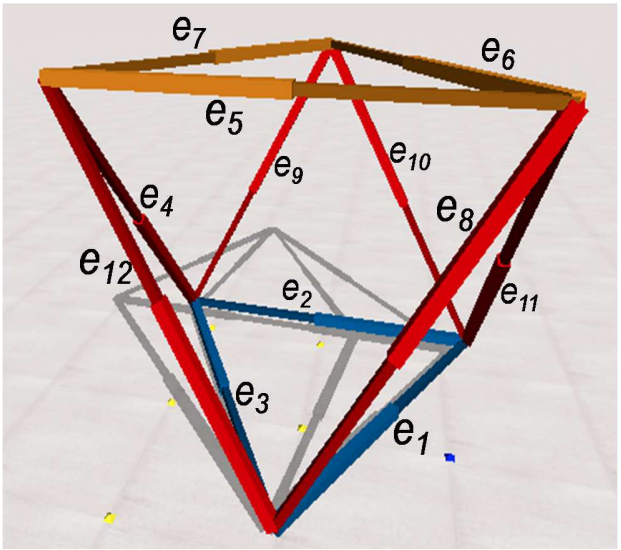

Figure 3: Simulation model implemented using the Open Dynamics Engine. The twelve linear actuators are shown at the edges $\{e_1,\ldots e_{12}\}$ of the platform.

Analysis of Deformation Modes

To begin studying the locomotion capabilities of the octahedron robot, we analyze different deformations by looking at the amount of power required by linear actuators to sustain different configurations at steady state. The octahedron is a highly redundant over-actuated system, and it is natural to expect that some motor commands will over stress the structure, due to antagonistic force patterns that propagate along the structure. Furthermore, it is important to identify the group of natural deformations that require a minimum amount of sustaining power, allowing for graceful motion.

The understanding of the force requirements of different deformation modes will enable the promotion of natural modes during locomotion, as well as the avoidance of antagonistic modes that can eventually harm the structure and drain excessive power. In addition, a good understanding of the force patterns that arise due to intrinsic actuation, might serve to identify patterns that can be only explained by interaction with the environment.

We note a commanded deformation by a row vector **c** (eq. (1) of twelve target reference positions $\{r_1,\ldots r_{12}\}$ for the linear actuators $\{e_1,\ldots e_{12}\}$ shown in Figure 3, so that r_i is the reference position for the actuator at edge e_i. Another convenient representation is a 4x3 matrix C that groups motion relevant segments in rows (eq. (2). This notation allows identifying the symmetries exploited by different deformations.

$$c = [r_1\ r_2\ r_3\ r_4\ r_5\ r_6\ r_7\ r_8\ r_9\ r_{10}\ r_{11}\ r_{12}] \quad (1)$$

$$C = \begin{bmatrix} r_5 & r_6 & r_7 \\ r_{11} & r_{10} & r_9 \\ r_4 & r_{12} & r_8 \\ r_1 & r_2 & r_3 \end{bmatrix} \quad (2)$$

Some natural deformation modes, that can be intuitively derived, are shown in Figure 4. The canonical configuration is shown in Figure 4a. We can describe this mode by

$$c_0 = [0\ 0\ 0\ 0\ 0\ 0\ 0\ 0\ 0\ 0\ 0\ 0] \quad (3)$$

Global expansion and contraction (Fig. 4b, c) of the platform might be important for adapting to the different sizes of a given cavity. This mode can be represented by

$$c_1 = \alpha \cdot [1\ 1\ 1\ 1\ 1\ 1\ 1\ 1\ 1\ 1\ 1\ 1] \quad (4)$$

Where α is the scaling constant that modulates the deformation. Expansion of a single face allows anchoring on the cavity surface with just three edges (Figure 4d, e). Examples of face expansion modes are:

$$c_2 = \alpha \cdot [1\ 1\ 1\ 0\ 0\ 0\ 0\ 0\ 0\ 0\ 0\ 0] \quad (5)$$

$$c_3 = \alpha \cdot [0\ 0\ 0\ 0\ 1\ 1\ 1\ 0\ 0\ 0\ 0\ 0] \quad (6)$$

Relative rotation of parallel faces (Figure 4f) allows further adaptation of the platform to the cavity internal geometry.

$$c_4 = \alpha \cdot [0\ 0\ 0\ 1\ 0\ 0\ 0\ 1\ 0\ 1\ 0\ 0] \quad (7)$$

Extension of the robot orthogonal to the anchoring faces is another fundamental mode of locomotion (Figure 4g) since it allows transitioning from different anchoring points, corresponding to the extension phase of peristaltic motion.

$$c_5 = \alpha \cdot [0\ 0\ 0\ 1\ 0\ 0\ 0\ 1\ 1\ 1\ 1\ 1] \quad (8)$$

Rotation of one face place with respect to its counter face is another natural mode of motion that might be used for accessing branches of a tunneling structure or cavity.

$$c_6 = \alpha \cdot [0\ 0\ 0\ 0\ 0\ 0\ 0\ 1\ 0\ 0\ 1\ 0] \quad (9)$$

Continuing this analysis might lead to the identification of various other natural modes that can be useful for locomotion of the structure. However, we would like to discover and characterize automatically the different motion modes of the octahedron structure. We present in the next section a method for the characterization of motion modes for highly over actuated structures.

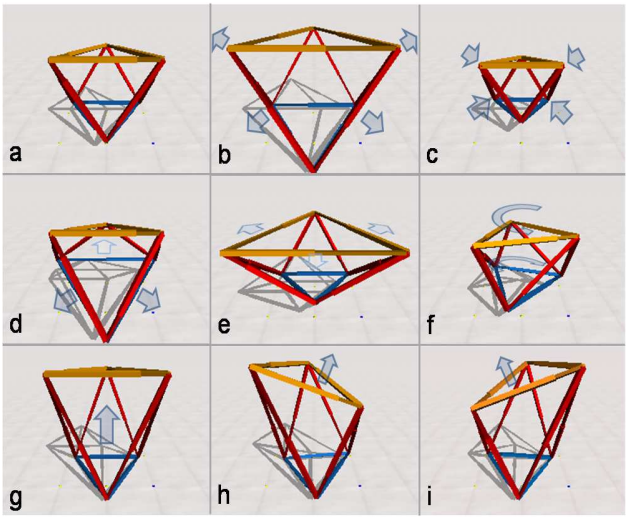

Figure 4: Example of some natural modes of deformation of the octahedral platform. a, Canonical configuration. **b**, Equilateral expansion. **c**, Equilateral contraction. **d**, Expansion of base face. **e**, Expansion of top face. **f**, Rotation relative to base and top faces. **g**, Face relative extension. **h**, Rotation of one counter face relative to the other. **i**, Same as in h but in another direction.

Automatic Characterization of Deformation Modes

Force feedback signals resulting from linear actuators can be used to sense characteristics of the surrounding environment touched by the robot (geometry, roughness, stiffness, etc.). Sensing the intrinsic distribution of forces might be useful for locomotion and shape shifting. The interpretation of force patterns might serve to minimize global energy consumption, preserve adequate levels of stress along the structure, and even sense structural damage.

Due to the complexity of the robot, motor commands might produce over stress and even harm the structure. Eventually a controller might incorporate force feedback as a means for smooth locomotion of the machine along a cavity or pipe.

The physical simulation of the octahedron robot allows us to rapidly test force distributions resulting from any commanded deformation. We have decided to exploit this advantage by testing a large set of deformations. This set is defined by all possible deformations that can be obtained by expanding or not, by a small amount $\alpha = \varepsilon$, each linear actuator. This results in a total of $|c| = 2^{12} = 4096$ possible deformations to be evaluated.

We analyzed each deformation starting with the robot under the canonical configuration c_0, then, we commanded a deformation vector c_T at time $t = 0$, and we computed the total power applied by the linear actuators at evaluation time $t = 100s$. The idea was to check the amount of power required to sustain c_T during steady state. Since each linear actuator carries its own PID dynamic compensator, the amount of power is proportional to the overall force resulting over the edge as a consequence of the intrinsic actuation.

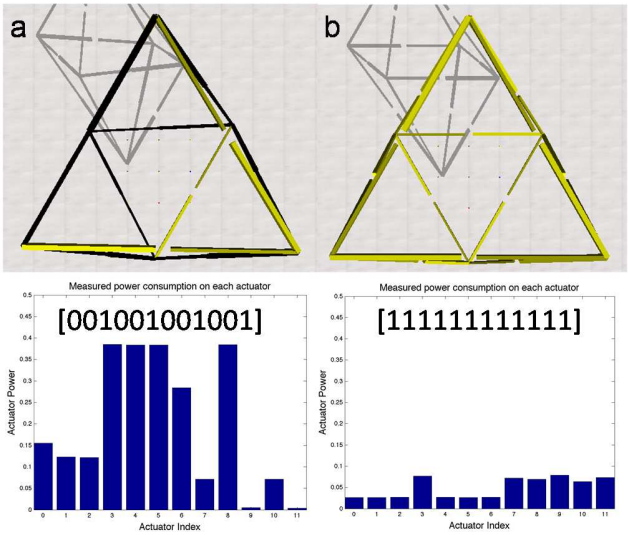

Figure 5: Power consumption measured on each linear actuator. Edges having a positive target (expanding) are shown in yellow. Those with extension target equal to zero are shown in black. **a**, A non-natural deformation. **b**, Equilateral expansion.

To ensure that forces are only intrinsic, due to the internal compensation required to sustain the target deformation, as well as to the properties of the octahedron geometry, we lifted the octahedron from ground and we set gravity to zero. Figure 6 shows plots of the total power that resulted for each deformation tested. Results appear sorted in ascending **(a)** and descending **(b)** order of total power.

These results are interesting, since they allow identifying groups of deformations having similar power consumptions. Moreover, one can easily note three groups of data, namely the natural deformations characterized by low energy

consumption (blue ellipse), an intermediate group of deformations (gray ellipse), and a set of deformations characterized by high power consumption (red ellipse).

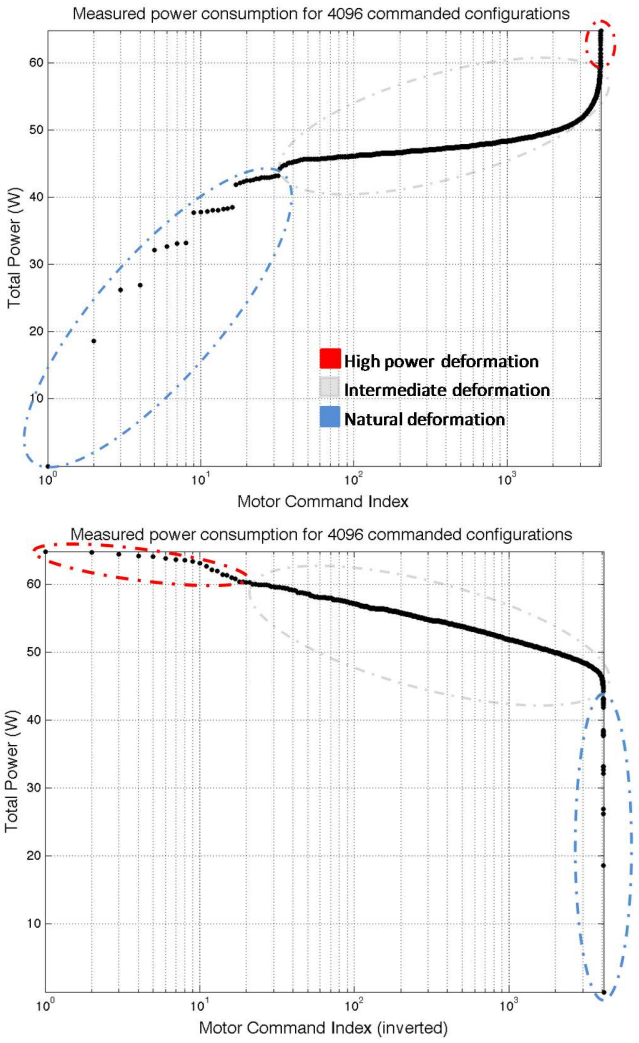

Figure 6: Total power consumption required by each commanded deformation under analysis. Results are shown in ascending order (top) and descending order (bottom) of total power consumption. A proposed distinction between high power, intermediate and natural deformation is indicated with dashed ellipses.

Evolving Basic Locomotion Modes

Several control strategies can be applied for commanding such a redundant, over actuated platform. A model based approach would require a geometrical representation describing the space of deformations that preserve the structure. The method described in previous section is a step toward obtaining such representation. Shape shifting under the above mentioned natural modes of deformation is in general consistent with the remainder of the structure and therefore it requires small amounts of energy and force.

We first studied locomotion inside a simulated pipeline. A peristaltic locomotion controller was intuitively defined by six phases of motion, corresponding to: (1) expansion of the front face c_3, (2) contraction of rear face c_2, (3) contraction of c_5 edges, (4) expansion of rear face c_2, (5) contraction of front face c_3, and (6) extension of c_5 edges.

We defined a space of controller solutions with the parameters of maximum edge extension l_{max}, and duration of each motion phase $\{\tau_1, \tau_2, \tau_3, \tau_4, \tau_5, \tau_6\}$. We used a simple genetic algorithm to search the space of possible solutions. A genome was represented by the vector $g = \{l_{max}, \tau_{3\text{-}6}, \tau_1, \tau_2, \tau_4, \tau_5\}$. To enforce peristaltic symmetry, we used the same duration ($\tau_{3\text{-}6}$) for the phases of contraction and expansion of of c_5 edges.

Crossover was performed with a probability P_c = 0.8 and mutation with a probability P_m = 0.01. After nearly 100 generations we obtained a ~40% of speed increase with respect to the starting engineered solution. The population size was set to 20 individuals. Figure 7 shows different stages of vertical locomotion inside a simulated straight pipe.

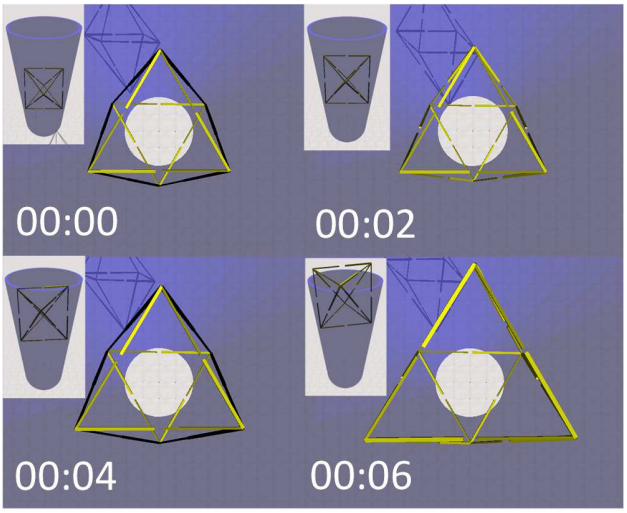

Figure 7: Simulation of octahedron platform traveling inside a vertical pipe. The robot is able to climb up the pipe interior while executing the peristaltic controller.

Navigation along {L,T,Y}-shaped pipelines

Many in-pipe robots are able to navigate along horizontal straight pipelines [19]. However, some pipeline configurations are particularly challenging for these machines. This is the case of pipeline branches and elbows.

A main problem is due to the internal geometrical changes that a robot faces when moving along these structured cavities. Figure 8 shows the group of nine pipe-joints that we have selected to test the motion capabilities of the octahedron platform.

We have considered L-shaped, T-shaped and Y-shaped joints of varying degrees of smoothness. The joint smoothness increases toward the right hand side of the figure. A dashed arrow on the left indicates the target robot trajectory on each pipe-joint.

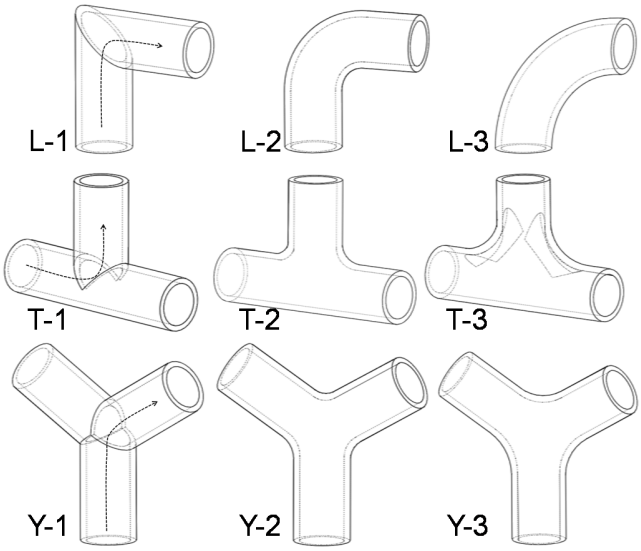

Figure 8: Pipeline elbows and branches used for testing the motion capability of the octahedron robot. We used L-shaped, T-shaped and Y-shaped pipeline joints with three different degrees of smoothness (increasing toward the right). The target robot path is shown with a dashed arrow on the left.

We carried out ten simulation trials per joint. During each trial, the experimenter was able to switch the orientation of peristaltic motion to be either lateral or vertical. This was particularly useful for motion inside T-shaped joints.

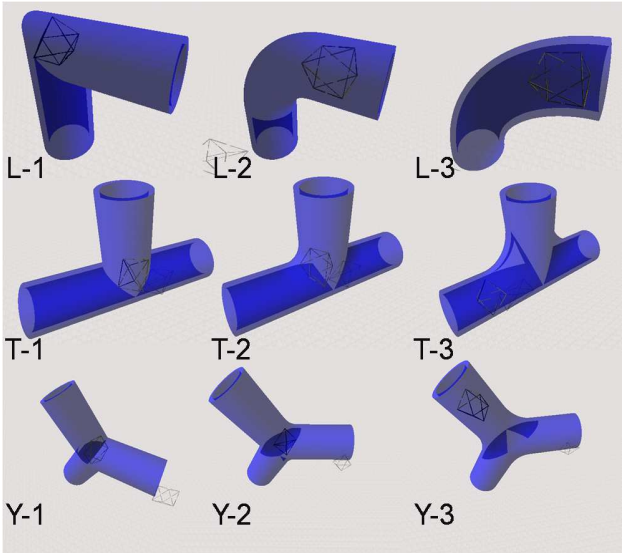

Figure 9: Screenshots taken during each joint simulation. The octahedron is shown while following the target path indicated in previous figure.

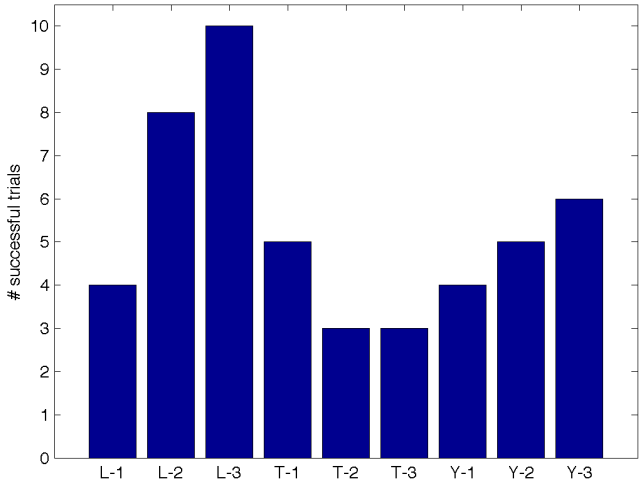

Figure 10: Number of successful trials out of a 10-trial test run. Results are shown for each joint under analysis.

A trial was counted as successful if the experimenter was able to drive the robot along the corresponding target path within a limited period of 15 *s*. Figure 9 shows screenshots of motion evaluation trials. The resulting number of successful trials per joint is shown in Figure 10.

The robot was able to travel along the target path one every joint. The resulting number of successful trials is not yet a statistically relevant indicator, but it allows us to identify L-3 as the joint that can be most easily surpassed. The joints L-1, T-2, T-3 and Y-1 appear as the most difficult to surpass.

Real Robots

We implemented the octahedron robotic concept with two real prototypes; the first is a hydraulic robot that uses syringes as linear actuators. A board of syringes is used for manual actuation. This robot is presented in Figure 11. We also performed locomotion experiments which are shown in Figure 12. The device was able to move at nearly one meter per minute when manually actuated.

We also built an electrically actuated robot which is shown in Figure 1, at the beginning of this paper. Both devices are tethered. The operation of the hydraulic device was aided by the force feedback transmitted along the water filled lines. We are currently working toward obtaining force feedback signals from the electrically actuated robot.

Figure 13 shows design details of the implemented electric linear actuators. A longitudinal cut of the actuator is presented together with an exploded view showing the different components.

It is important to mention that the construction was possible thanks to the use of a laser cutter. Some parts were machined using classical methods, although they can be easily fabricated with 3D printing. Figure 14 shows shape shifting tests performed with the electric prototype.

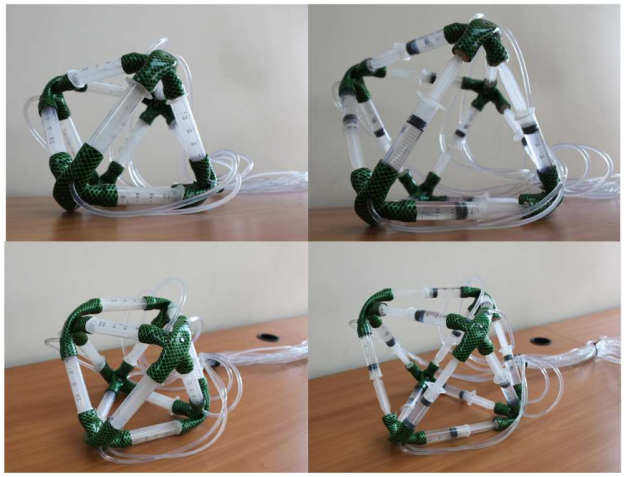

Figure 11: Hydraulic prototype constructed using syringes. The prototype is remotely actuated manually.

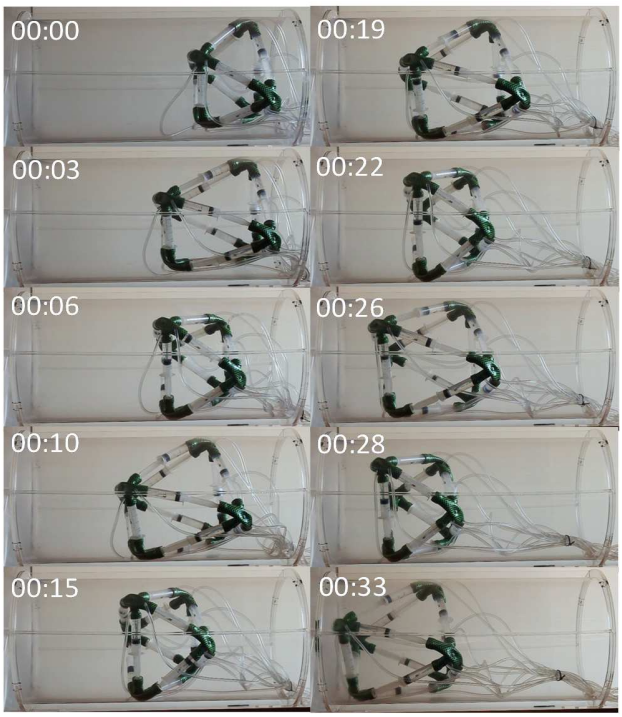

Figure 12: Locomotion inside a real pipe, ~60 *cm* length. The peristaltic controller was applied on a real setup showing succesfull lateral motion.

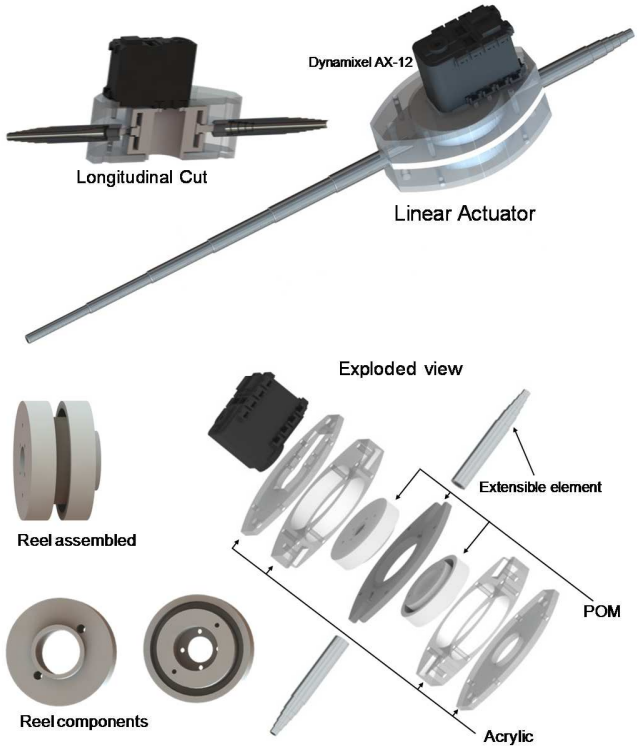

Figure 13: Different views of the design and components used for the construction of the electric linear actuators. The robot can be easily reproduced using digital fabrication techniques, such as laser cutting and 3D printing.

Conclusions

We have shown how an octahedron robot is able to travel under confinement. The robot is able to navigate along different simulated {L,T,Y}-shaped pipe joints. We have evolved a motion controller for the lateral displacement of this new robotic platform. In addition, we have presented a method to automatically explore and characterize structural deformations in terms of energy consumption. Using this method we have detected three groups of deformations which are defined by either low (natural), intermediate and high power demands. Eventually, a sense of touch might be derived from a thorough understanding of force feedback signals of the octahedral structure.

Acknowledgements

This research was funded by Fondecyt project number 11110353. We thank the thorough and detailed revision provided by anonymous reviewers.

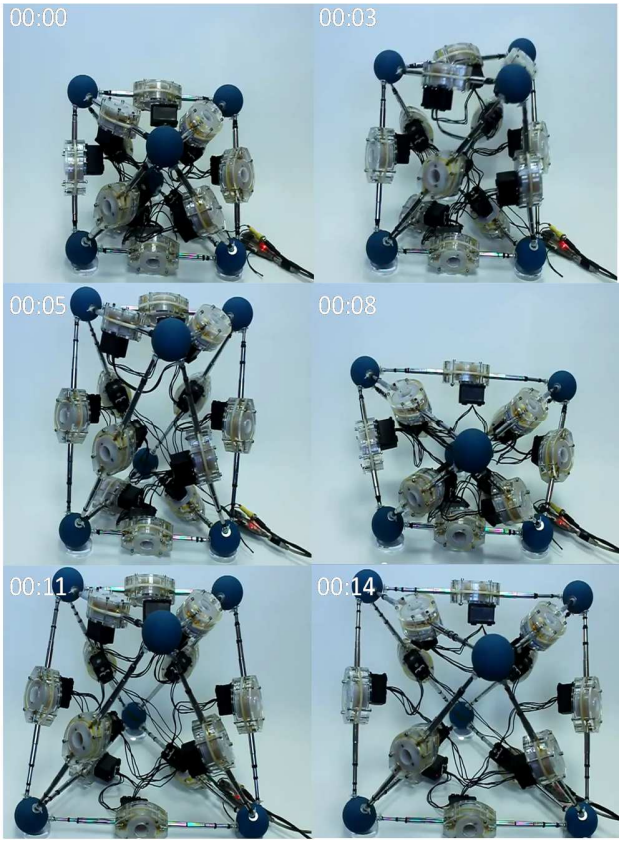

Figure 14: Illustration of shape shifting capabilities of the electric prototype. Natural modes of deformation were tested.

References

1. Abrahantes, M., Silver, A. and Wendt, L. (2007). Gait design and modeling of a 12-tetrahedron walker robot. In *Thirty-Ninth Southeastern Symposium on System Theory*, pages 21–25. IEEE, Macon, GA.
2. Abrahantes, M., Nelson, L. and Doorn, P. (2010). Modeling and Gait Design of a 6-Tetrahedron Walker Robot. In *42nd Southeastern Symposium on System Theory*, pages 248–252. IEEE, Tyler, TX.
3. Correll, N., Onal, C. D., Liang, H., Schoenfeld, E., & Rus, D. (2010). Soft Autonomous Materials — Using Active Elasticity and Embedded Distributed Computation. *12th International Symposium on Experimental Robotics*. New Delhi, India.
4. Curtis, S., Brandt, M., Bowers, G., Brown, G., Cheung, C., Cooperider, C., Desch, M., et al. (2007). Tetrahedral Robotics for Space Exploration. *IEEE Aerospace and Electronic Systems Magazine*, *22*(June), 22-30.
5. Davis, A. (2002). Urban search and rescue robots: from tragedy to technology. *IEEE Intelligent Systems*, 17(2):81–83.
6. de Jager, B., & Skelton, R. E. (2005). Input-output selection for planar tensegrity models. *Control Systems Technology, IEEE Transactions on*, *13*(5), 778–785.
7. Fest, E., Shea, K., & Smith, I. (2004). Active tensegrity structure. *Journal of Structural Engineering*, *130*(October), 1454-1465.
8. Gayle, R., Lin, M.C. and Manocha, D. (2005). Constraint-based motion and planning of deformable robots. In *Proceedings of the 2005 IEEE International Conference Robotics and Automation*, pages 1046–1053. Barcelona, Spain.
9. Gayle, R. and Segars, P. and Lin, M.C. and Manocha, D. (2005b). Path planning for deformable robots in complex environments. In *Proceedings of the Robotics Science and Systems Conference (RSS)*, pages 225–232. Cambridge, MA.
10. Lyder, A., Garcia, R., & Stoy, K. (2008). Mechanical design of Odin, an extendable heterogeneous deformable modular robot. *Intelligent Robots and Systems, 2008. IROS 2008. IEEE/RSJ International Conference on* (pp. 883–888).
11. Mangan, E. V., Kingsley, D. A., Quinn, R. D., & Chiel, H. J. (2002). Development of a peristaltic endoscope. *Robotics and Automation, 2002. Proceedings. ICRA'02. IEEE International Conference on (Vol. 1, pp. 347–352). IEEE.*
12. Nakamura, T., Kato, T., & Iwanaga, T. (2006). Development of a Peristaltic Crawling Robot Based on Earthworm Locomotion. *Journal of Robotics and Mechatronics*, 18(3), 299-302.
13. Nakamura, T. (2008). Locomotion and turning patterns of a peristaltic crawling earthworm robot composed of flexible units. 2008 IEEE/RSJ International Conference on Intelligent Robots and Systems (pp. 1630-1635).
14. Paul, C. and Valero-Cuevas, F.J. and Lipson, H. (2006). Design and control of tensegrity robots for locomotion. *IEEE Transactions on Robotics*, 22(5):944–957.
15. Pfeifer, R., Iida, F. (2005). Morphological computation: Connecting body, brain and environment. *Japanese Scientific Monthly*, 58(2), 48–54.
16. Quillin, K. (1999). Kinematic scaling of locomotion by hydrostatic animals: ontogeny of peristaltic crawling by the earthworm lumbricus terrestris. Journal of Experimental Biology, 202 (Pt 6)(6), 661-74
17. Rieffel, J., Trimmer, B., & Lipson, H. (2008). Mechanism as Mind: What Tensegrities and Caterpillars Can Teach Us about Soft Robotics. *Artificial Life XI: Proceedings of the Eleventh International Conference on the Simulation and Synthesis of Living Systems* (pp. 506-512). Winchester, U.K.: MIT Press, Cambridge, MA.
18. Rieffel, J.A. and Valero-Cuevas, F.J. and Lipson, H. (2010). Morphological communication: exploiting coupled dynamics in a complex mechanical structure to achieve locomotion. *Journal of the Royal Society Interface*, 45(7):1742–5689.
19. Roh, S. and Choi, H.R. (2005). Differential-drive in-pipe robot for moving inside urban gas pipelines. *IEEE Transactions on* Robotics, 21(1):1552–3098.
20. Saga, N., & Nakamura, T. (2004). Development of a peristaltic crawling robot using magnetic fluid on the basis of the locomotion mechanism of the earthworm. *Smart Materials and Structures*, 13(3), 566-569.
21. Seok, S., Onal, C. D., Wood, R., Rus, D., & Sangbae, K. (2010). Peristaltic locomotion with antagonistic actuators in soft robotics. *IEEE International Conference on Robotics and Automation (ICRA)* (Vol. 60).
22. Sugiyama, Y. (2004). Crawling and jumping of deformable soft robot. *Proceedings of 2004 IEEE/RSJ International Conference on Intelligent Robots and Systems* (pp. 3276-3281). Sendai, Japan.
23. Skelton, R. (2001). Dynamics of the shell class of tensegrity structures. *Journal of the Franklin Institute*, *338*(2-3), 255-320.
24. Trimmer, B.A. and Takesian, A.E. and Sweet, B.M. and Rogers, C.B. and Hake, D.C. and Rogers, D.J. (2006). Caterpillar locomotion: A new model for soft-bodied climbing and burrowing robots. In *Proceedings of the 7th International Symposium on Technology and the Mine Problem*, Monterey, CA.